THRESHOLD OF FRONT PROPAGATION IN NEURAL FIELDS: AN INTERFACE DYNAMICS APPROACH

GRÉGORY FAYE* AND ZACHARY P. KILPATRICK†

Abstract. Neural field equations model population dynamics of large-scale networks of neurons. Wave propagation in neural fields is often studied by constructing traveling wave solutions in the wave coordinate frame. Nonequilibrium dynamics are more challenging to study, due to the nonlinearity and nonlocality of neural fields, whose interactions are described by the kernel of an integral term. Here, we leverage interface methods to describe the threshold of wave initiation away from equilibrium. In particular, we focus on traveling front initiation in an excitatory neural field. In a neural field with a Heaviside firing rate, neural activity can be described by the dynamics of the interfaces, where the neural activity is at the firing threshold. This allows us to derive conditions for the portion of the neural field that must be activated for traveling fronts to be initiated. Explicit equations are possible for a single active (superthreshold) region, and special cases of multiple disconnected active regions. The dynamic spreading speed of the excited region can also be approximated asymptotically. We also discuss extensions to the problem of finding the critical spatiotemporal input needed to initiate waves.

Key words. neural field equations, traveling fronts, propagation threshold, interface equations

1. Introduction. Traveling waves are ubiquitous in nature, arising in a wide variety of biological processes, including epidemics [26], actin polymerization [1], and evolution [38]. These processes are usually modeled by nonlinear partial differential equations (PDE) that combine nonlinear local interactions and spatial dynamics like diffusion [35]. Such continuum equations can yield traveling wave solutions in closed form, so the effect of model parameters on wave dynamics can be quantified in detail. For instance, neural field models describe large-scale dynamics of nonlocally connected networks of neurons, and their constituent functions can be tuned to produce a multitude of spatiotemporal solutions [7]. Such results can be connected to coherent neural activity patterns observed in cortical slice and in vivo experiments [28, 29, 37].

Large-scale neural activity imaged using voltage sensitive dye exhibits myriad forms of propagating neural activity in different regions of the brain [41, 43]. For instance, sensory inputs can nucleate traveling waves in olfactory [16] and visual cortices [27]. Waves may propagate radially outward from the site of nucleation [23], with constant direction as plane waves [44], or rotationally as spiral waves [29]. Sufficiently large amplitude sensory stimuli can initiate traveling waves of neural activity, but the threshold for initiation is difficult to identify [39]. A recent study has shown that if two visual stimuli are presented sufficiently close together in time, only a single wave is generated [25]. This suggests there is an internal state-dependent threshold that shapes the time and stimulus-amplitude necessary for wave initiation. In this work, we analyze a neural field model to understand how such propagation thresholds can be defined in a large-scale network of neurons.

Neural field equations provide a tractable model of coherent neural activity, which can be used to relate features of a network to the activity patterns it generates [7, 9]. The building blocks of a neural field are excitatory neurons, which activate their neighbors, and inhibitory neurons, which inactivate their neighbors. Wilson and Cowan showed that a localized stimulus to an excitatory/inhibitory neural field can pro-

---
*CNRS, UMR 5219, Institut de Mathématiques de Toulouse, 31062 Toulouse Cedex, France (`gregory.faye@math.univ-toulouse.fr`)

†Department of Applied Mathematics, University of Colorado, Boulder, Colorado 80309, USA (`zpkilpat@colorado.edu`). This author is supported by NSF grant (DMS-1615737).

duce outward propagating traveling waves [42], and Amari constructed such solutions assuming a high gain firing rate function [2]. Following this seminal work, Ermentrout and McLeod used a continuation argument to prove the existence of traveling fronts in a purely excitatory neural field [19]. Subsequent studies of neural fields have built on this work by incorporating propagation delays or spatial heterogeneity and by adding variables representing slow processes like adaptation [20, 21, 30, 31, 36]. A wide variety of spatiotemporal patterns emerge including Turing patterns [8], traveling pulses [12, 22, 36], breathers [24], and self-sustained oscillations [31, 40]. However, most previous work focuses on construction of solutions and local dynamics near equilibria, addressed via linear stability or perturbation theory [13, 30, 34]. Nonequilibrium dynamics are less tractable in these infinite-dimensional systems, and so there are few results exploring the outermost bounds of equilibrium solutions' basins of attraction.

In the present study, we characterize the basins of attraction of the stationary solutions of an excitatory neural field. We focus on a scalar neural field model that supports traveling front solutions [19, 36]:

$$
(1) \quad
\begin{cases}
\partial_t u(x,t) = -u(x,t) + \int_{\mathbb{R}} w(x-y) H(u(y,t) - \kappa) \mathrm{d}y + I(x,t), & t > 0, \quad x \in \mathbb{R}, \\
u(x,0) = u_0(x), & x \in \mathbb{R},
\end{cases}
$$

where $u(x,t)$ is the total synaptic input at location $x \in \mathbb{R}$ and time $t > 0$ and $w(x-y)$ is a kernel describing synaptic connections from neurons at location y to those at x. Our results can be extended to the case $x \in \mathbb{R}^2$, as we will show in a subsequent paper. We assume the kernel $w(x)$ is even, $w(x) = w(-x)$; decreasing in $|x| > 0$; positive, $w(x) > 0$; and has a bounded integral, $\int_{\mathbb{R}} w(x) \mathrm{d}x < \infty$. For simplicity, we consider a normalized kernel $\int_{\mathbb{R}} w(x) \mathrm{d}x = 1$, but this is not necessary. To calculate explicit results, we consider the exponential kernel [6, 36]

$$
(2) \quad w(x) = \frac{1}{2} \mathrm{e}^{-|x|}.
$$

Nonlinearity in Eq. (1) arises due to the Heaviside firing rate function [13, 19]

$$
H(u - \kappa) = \begin{cases} 1, & u \geq \kappa, \\ 0, & u < \kappa, \end{cases}
$$

allowing us to determine dynamics of Eq. (1) by the threshold crossings $u(x_j(t), t) = \kappa$, yielding interface equations [10, 15]. Note, the analysis presented herein relies strongly on the assumption of a step nonlinearity, but see [14] for methods of approximating wave solutions in neural fields with steep sigmoid nonlinearities, which could be extended to the derive interface equations.

Our analysis focuses on the case of Eq. (1) for which traveling fronts propagate outward, so active regions $(u(x,t) \geq \kappa)$ invade inactive regions $(u(x,t) < \kappa)$. As a consequence, throughout the manuscript we assume $\kappa \in (0, 1/2)$. We derive this condition explicitly in Section 2. The central focus of our work is to examine how the long term dynamics of Eq. (1) are determined by the initial condition $u(x,t) = u_0(x)$. For simplicity, we restrict $0 \leq u_0(x) \leq 1$, $\forall x \in \mathbb{R}$. We also examine the impact of external inputs $I(x,t)$, determining how they shape the long term behavior of Eq. (1).

Several previous studies have shown that traveling front solutions to Eq. (1) can be constructed [6, 19, 36]. Importantly they coexist with the two stable homogeneous states, $u \equiv 0$ and $u \equiv 1$. Thus, some initial conditions $u_0(x)$ will decay $(u \to 0)$, but others will propagate $(u \to 1)$ as $t \to \infty$. Our work addresses the following question:

What conditions on $u_0(x)$ and Eq. (1) determine $\lim_{t \to \infty} u(x, t)$? Note, in Section 2, we explicitly construct a family of unstable intermediate stationary solutions, including single bumps and periodic patterns. While it is tempting to consider these solutions separatrices between the quiescent state ($u \equiv 0$) and the emergence of two counter-propagating fronts, this picture of the full dynamics of Eq. (1) is incomplete. One can easily construct initial conditions $u_0(x)$ whose long term dynamics cannot be resolved by simply examining properties of these intermediate solutions. A related point is that intuition gained from analyzing the equivalent problem in nonlinear PDE models (whose interactions are local) [17, 45] does not readily extend to the analysis of neural fields (which are nonlocal). To distinguish cases that lead to decay versus propagation, we project the neural field Eq. (1) dynamics to equations for the interfaces $x_j(t)$ where $u(x_j(t), t) = \kappa$.

Our paper proceeds as follows. In Section 2, we summarize the classes of entire solutions to Eq. (1), which are relevant for our analysis, noting there are (i) homogeneous states, $u(x, t) \equiv \bar{u} \in \{0, 1\}$; (ii) a family of unstable stationary solutions, $u(x, t) = U_L(x)$ with period L; and (iii) traveling waves, $u(x, t) = U_f(x - ct)$. Next, in Section 3, we analyze the nonequilibrium dynamics of Eq. (1) using interface equations for the case in which $u_0(x) \geq \kappa$ on a single active region $x \in [x_1, x_2]$, which allows us to classify the threshold between propagation ($u \to 1$) and failure ($u \to 0$). Our reduced interface equations also allow us to calculate the timescale of the transient dynamics as they approach equilibrium. In addition, we discuss requirements on an external stimulus $I(x, t)$ necessary to activate a traveling wave. In Section 4, we derive interface equations for Eq. (1) for multiple ($N > 1$) active regions $u_0(x)$ for $x \in \cup_{n=1}^{N} [x_{2n-1}, x_{2n}]$. Some explicit results are possible in the cases $N \to \infty$ and $N = 2$, showing interactions between active regions impact the propagation threshold. Our analysis provides a tool for linking initial conditions of spatially-extended neural field equations away from equilibrium to their eventual equilibrium state.

2. Entire solutions of the excitatory neural field. We begin by summarizing the relevant entire solutions of the neural field Eq. (1) for $I(x, t) \equiv 0$. By entire solutions, we mean solutions of Eq. (1) which are defined for all time $t \in \mathbb{R}$, which includes traveling waves and three types of stationary solutions:

   (i) the two homogeneous states $u = 0$ and $u = 1$, which are both locally stable;
   (ii) an unstable symmetric one bump solution U_b;
   (iii) a family of periodic solutions U_L which are all unstable.

Homogeneous states (i) are locally stable, attracting almost all initial conditions (Fig. 1A,B), whereas the other stationary states separate some initial conditions (ii,iii) into those that propagate and those that decay (Fig. 1B). However, multimodal initial conditions cannot be characterized using local analysis (Fig. 1C). Our analysis in Sections 3 and 4 will emphasize the nonequilibrium dynamics away from entire solutions, exploring conditions necessary for attraction to one of the two homogeneous states. Traveling waves and stationary solutions have been characterized in detail in previous works, so we will simply state key formulas rather than carrying out derivations [2, 5, 7, 9, 11, 18, 24, 32].

2.1. Bump solution. Stationary bumps $u(x, t) = U_b(x)$, with a single active region $U_b(x) \geq \kappa$ for $x \in [x_1, x_2]$, centered at $x = 0$, so $x \in [-b, b]$ take the form

$$(3) \qquad U_b(x) = \int_{-b}^{b} w(x - y) \mathrm{d}y = W(x + b) - W(x - b),$$
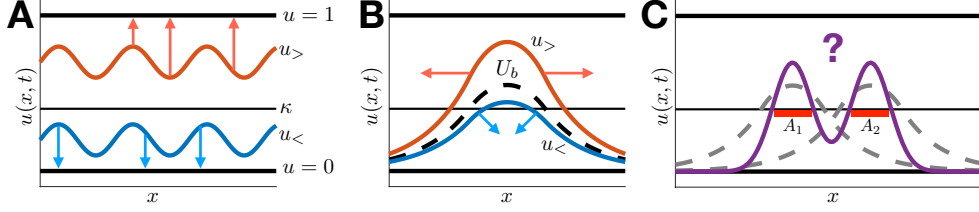
FIG. 1. *Long term behavior of initial conditions $u_0(x)$ for Eq. (1) in 1D. (A) Entirely sub-threshold (superthreshold) initial conditions decay (grow). If $u_0(x) < \kappa$, $\forall x$, then $u \to 0$ as $t \to \infty$ ($u_<$), whereas if $u_0(x) \geq \kappa$, $\forall x$, then $u \to 1$ as $t \to \infty$. (B) Initial conditions below (above) the unstable bump $U_b(x)$ decay (grow). If $u_0(x) < U_b(x)$, $\forall x$, then $u \to 0$ as $t \to \infty$ ($u_<$), whereas if $u_0(x) > U_b(x)$, $\forall x$, then $u \to 1$ as $t \to \infty$. (C) Characterization of $\lim_{t\to\infty} u(x,t)$ is less straightforward for multimodal initial conditions. Even though each active region (A_1 and A_2, where $u_0(x) \geq \kappa$) is narrower than the unstable bump $U_b(x)$, this initial condition could lead to propagation due to nonlocal interactions.*

where we have defined the antiderivative of the weight kernel

$$(4) \qquad W(x) = \int_0^x w(y) \mathrm{d}y.$$

The threshold condition $U_b(\pm b) = W(2b) = \kappa$ can be solved to identify the unique bump half-width b: $b_0(\kappa) = W^{-1}(\kappa)/2$ for any $\kappa \in (0, 1/2)$. Local stability analysis can be used to show U_b is linearly unstable [2, 24].

2.2. Periodic solutions. There are also L-periodic stationary solutions $U_L(x)$ with an infinite number of superthreshold regions $\cup_{n=-\infty}^{\infty}[-b+nL, b+nL]$, under the restriction $2b < L$, which take the form [32]

$$(5) \qquad U_L(x) = \sum_{n\in\mathbb{Z}} \int_{-b+nL}^{b+nL} w(x-y)\mathrm{d}y = \sum_{n\in\mathbb{Z}} \left(W(x+b+nL) - W(x-b+nL)\right).$$

Applying any threshold condition, $U_L(\pm b + nL) = \kappa$, we obtain an implicit equation for the region half-widths b given by

$$(6) \qquad \kappa = \sum_{n\in\mathbb{Z}} \left(W(2b+nL) - W(nL)\right) := \mathbf{W}_L(b),$$

which can be inverted for $\kappa \in (0,1)$ and $L > 0$, to obtain the unique solution

$$b_L(\kappa) = \mathbf{W}_L^{-1}(\kappa) \in (0, L/2).$$

A local analysis can be used to show that U_L is linearly unstable [32].

2.3. An illustrative example: exponential weight kernel. For an exponential weight kernel, Eq. (2), the Fourier transform of w is $\hat{w}(k) = 1/(1+k^2)$ for $k \in \mathbb{R}$, so convolution by w corresponds to the operator $(\mathrm{I}-\partial_{xx})^{-1}$. As a consequence, any stationary solutions of Eq. (1) are solutions of the piecewise-smooth second order differential equation, $U(x) - U''(x) = H(U(x) - \kappa)$, which can be written as

$$(7) \qquad \begin{cases} U'(x) &= V(x), \\ V'(x) &= U(x) - H(U(x) - \kappa). \end{cases}$$

The complete phase portrait of Eq. (7) is given in Fig. 2 from which we recover the existence of a unique symmetric bump solution and a family of periodic solutions.
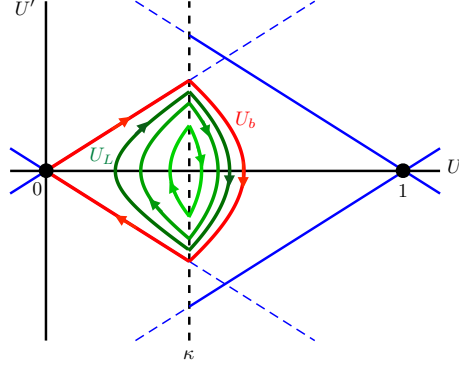
4

FIG. 2. *Phase portrait of Eq. (7), describing stationary solutions of Eq. (1) with an exponential kernel, Eq. (2) with $\kappa \in (0, 1/2)$. Solid black horizontal and blue diagonal lines are nullclines of U and U', respectively. Homogeneous states $\bar{U} = 0, 1$ occur at their intersection. Homoclinic orbits arise about the point $(U, U') = (\kappa, 0)$, crossing the threshold κ twice. The single bump U_b (red outer trajectory) forms a separatrix, bounding all other nontrivial stationary solutions. There exists an infinite number of periodic solutions U_L inside (green inner trajectories), whose orbits shrink as L is decreased from infinity.*

2.4. Traveling fronts. To construct traveling wave solutions, we introduce the traveling wave coordinate $\xi = x - ct$, where c denotes the wave speed, and integrate the corresponding equation to yield [6, 13, 36]

$$U_f(\xi) = e^{\xi/c} \left[\kappa - \frac{1}{c} \int_0^\xi e^{-y/c}(W_\infty - W(y)) dy \right].$$

Assuming $c > 0$ (for $\kappa \in (0, 1/2)$) and requiring boundedness implies

$$(8) \qquad \kappa = \frac{1}{c} \int_0^\infty e^{-y/c}(W_\infty - W(y)) dy,$$

and so the traveling front solution will be of the form

$$(9) \qquad U_f(\xi) = \frac{1}{c} \int_0^\infty e^{-y/c}(W_\infty - W(y + \xi)) dy.$$

Eq. (8) relates the wavespeed c to the threshold κ and kernel $w(x)$, and can be rearranged along with integration by parts to yield a simpler implicit equation for c,

$$(10) \qquad \int_0^\infty e^{-y/c} w(y) dy = W_\infty - \kappa.$$

Since $W_\infty = 1/2$, Eq. (10) will only have a solution with corresponding $c \in (0, \infty)$ if $\kappa \in (0, 1/2)$, since the integral on the left hand side is positive and bounded from above by W_∞. Local stability has been studied previously [13], demonstrating the wave solution U_f is marginally stable to perturbations that shift its location.

This concludes our analysis of entire solutions to Eq. (1) in the case $I \equiv 0$. Guided by the fact that the homogeneous solutions $\bar{u} \equiv 0, 1$ are stable, and the intermediate bump $U_b(x)$ and periodic solutions $U_L(x)$ are unstable, we generally expect initial conditions $u_0(x)$ to either be attracted to $\bar{u} \equiv 0$ or $\bar{u} \equiv 1$ as $t \to \infty$. In the next section, we demonstrate a means of determining the fate of unimodal initial conditions using interface equations.

3. Nonequilibrium dynamics of a single active region. In this section, we identify conditions on $u_0(x)$ with a single active region ($u_0(x) \geq \kappa$ for $x \in [x_1, x_2]$), so the solution to Eq. (1) propagates (assuming $I(x,t) \equiv 0$). In what follows, we assume $0 \leq u_0(x) \leq 1$ is unimodal, $u_0'(x_0) = 0$ and $u_0'(x) \gtrless 0$ for $x \lessgtr x_0$, ensuring there are no more than two interfaces for $t > 0$. First, we derive results for even $u_0(x) = u_0(-x)$, and then extend to asymmetric $u_0(x)$. Initial conditions can be separated into subthreshold ones that lead to decay and superthreshold ones that lead to propagation. Lastly, we identify conditions on the external input $I(x,t)$ to Eq. (1) that ensure propagation when $u_0(x) \equiv 0$.

3.1. Interface equations and criticality: even symmetric case. Symmetry of Eq. (1) with $I \equiv 0$ ensures solutions with even initial conditions are always even, so the active region $A(t) = \{x \in \mathbb{R} \mid u(x,t) \geq \kappa\}$ is symmetric for $t > 0$. The dynamics of the symmetric active region $A(t) = [-a(t), a(t)]$ can be described with interface equations for the two points $x = \pm a(t)$ (See [2,15]). We start by rewriting Eq. (1) as

$$
(11) \qquad \partial_t u(x,t) = -u(x,t) + \int_{A(t)} w(x-y) \mathrm{d}y,
$$

which can be further simplified:

$$
\partial_t u(x,t) = -u(x,t) + W(x+a(t)) - W(x-a(t)).
$$

Eq. (11) remains well defined even in the case where $a(t)$ vanishes. We can describe the dynamics of the two interfaces by the implicit equations

$$
(12) \qquad u(\pm a(t), t) = \kappa.
$$

Differentiating Eq. (12) with respect to t, we find the total derivative is:

$$
(13) \qquad \pm \alpha(t)a'(t) + \partial_t u(\pm a(t), t) = 0,
$$

where we define $a'(t) = \frac{\mathrm{d}a(t)}{\mathrm{d}t}$ and $\pm \alpha(t) = \partial_x u(\pm a(t), t)$. The symmetry of Eq. (13) allows us to reduce to a single differential equation for the dynamics of $a(t)$:

$$
(14) \qquad a'(t) = -\frac{1}{\alpha(t)} \left[W(2a(t)) - \kappa \right],
$$

where we have substituted Eq. (11) at $a(t)$ for $\partial_t u(a(t), t)$. Eq. (14) is not well-defined for $\alpha(t) = 0$, but we will show how to circumvent this difficulty. Furthermore, we can obtain a formula for $\alpha(t)$ by defining $z(x,t) := \partial_x u(x,t)$ and differentiating Eq. (11) with respect to x to find [15]

$$
\partial_t z(x,t) = -z(x,t) + w(x+a(t)) - w(x-a(t)),
$$

which we can integrate and evaluate at $a(t)$ to find

$$
(15) \qquad \alpha(t) = u_0'(a(t))\mathrm{e}^{-t} + \mathrm{e}^{-t} \int_0^t \mathrm{e}^s \left[w(a(t)+a(s)) - w(a(t)-a(s)) \right] \mathrm{d}s.
$$

Thus, we have a closed system describing the evolution of the right interface $a(t)$ of the active region $A(t)$, given by Eqs. (14) and (15), along with the initial conditions $a(0) = \ell$ and $\alpha(0) = u_0'(\ell) < 0$, as long as $\alpha(t) < 0$. Criticality occurs for initial
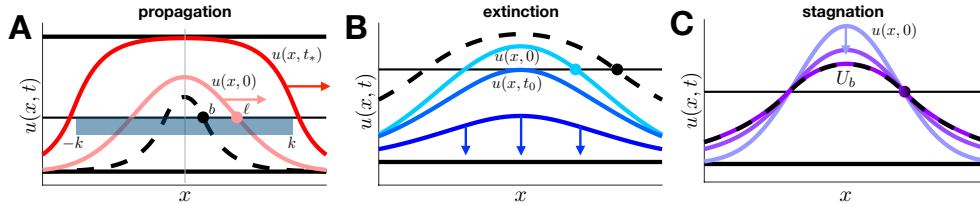
6

FIG. 3. *Long term behavior of $u(x,t)$ depends only on how the initial interface location $a(0) = \ell$ compares to the bump half-width, $b = W^{-1}(\kappa)/2$. (A) If $\ell > b$, propagation occurs and $\lim_{t\to\infty} u(x,t) \equiv 1$, $\forall x \in K = [-k,k]$ for $k < \infty$. This follows from the fact that for any K, we can find a time t_* for which $u(x,t_*) > \kappa$, $\forall x \in K$. (B) If $\ell < b$, eventually $u(x,t) < \kappa$, right after the time t_0 when $u(0,t_0) = \kappa$, and so $\lim_{t\to\infty} u(x,t) \equiv 0$. (C) If $\ell = b$, stagnation occurs and $\lim_{t\to\infty} u(x,t) = U_b(x)$.*

conditions such that $a'(t) = 0$, which means $W(2\ell) = \kappa$, *i.e.* for $\ell = b = W^{-1}(\kappa)/2$, so the critical ℓ is precisely the half-width of the unstable stationary bump solution $U_b(x)$ defined in Eq. (3).

Propagation. If $\ell > W^{-1}(\kappa)/2$ then $a'(t) > 0$ and, due to the monotonicity of w and Eq. (15), $\alpha(t) < 0$ for all time $t > 0$ so $\lim_{t\to\infty} a(t) = \infty$, and the active region $A(t)$ expands indefinitely. As a consequence, for any compact set $K = [-k,k]$ with $k > 0$ given and any $\epsilon > 0$, we can find $t_* > 0$ large enough such that $K \subset A(t_*)$ and

$$|W(x + a(t_*)) - W(x - a(t_*)) - 1| \le \epsilon, \quad \forall x \in K,$$

so that for any equal or later time $s \ge t_*$ we have

$$|W(x + a(s)) - W(x - a(s)) - 1| \le \epsilon, \quad \forall x \in K.$$

We can solve for $u(x,t)$ starting for time t_* to obtain

$$u(x,t) = u(x,t_*)e^{t_* - t} + e^{-t} \int_{t_*}^{t} e^s \left(W(x + a(s)) - W(x - a(s)) \right) \mathrm{d}s.$$

Using the fact that any solution is continuous, we have that $|u(x,t_*)| \le M$ for all $x \in K$. As a consequence, we get that $\forall x \in K$,

$$|u(x,t) - 1| = \left| (u(x,t_*) - 1)e^{t_* - t} + e^{-t} \int_{t_*}^{t} e^s \left(W(x + a(s)) - W(x - a(s)) - 1 \right) \mathrm{d}s \right|$$

$$\le (1 + M)e^{t_* - t} + \epsilon.$$

This implies that $\lim_{t\to\infty} |u(x,t) - 1| = 0$, $\forall x \in K$. As a consequence, the solutions of Eq. (1) locally uniformly converge to the homogeneous state $u \equiv 1$ as $t \to \infty$ (Fig. 3A). Thus, we have propagation of $u \equiv 1$ into $u \equiv 0$ as time evolves.

Extinction. If $\ell < W^{-1}(\kappa)/2$, then $a'(t) < 0$ and $0 < a(t) < \ell$ on $t \in (0, t_0)$. By continuity, there exists a finite $t_0 > 0$ such that $a(t_0) = 0$, at which point the interface dynamics, Eq. (14) and (15), breaks down. We know this because $W(2a(t)) - \kappa < 0$ and decreases as $a(t)$ decreases. Note also that for $t \in (0, t_0)$ we consistently have $\alpha(t) < 0$. Inspecting Eq. (15) shows that $\lim_{t\to t_0^-} \alpha(t) = 0$ since $u_0'(0) = 0$. Thus, at time $t = t_0$, we have $0 \le u(x, t_0) \le \kappa$, and for $t \ge t_0$, $\partial_t u(x,t) = -u(x,t)$, so $u(x,t) = e^{t_0 - t}u(x, t_0)$ for $t \ge t_0$, and $\lim_{t\to\infty} u(x,t) \equiv 0$, uniformly on $x \in \mathbb{R}$ (Fig. 3B).

7

Stagnation. If $\ell = W^{-1}(\kappa)/2$, then $a'(t) = 0$ for all time assuming $\alpha(t) < 0$, implying $a(t) \equiv \ell$. Plugging into Eq. (15) yields $\alpha(t) = (w(2b) - w(0))(1 - e^{-t}) + u_0'(\ell)e^{-t} < 0$ for $t > 0$. As a consequence, $a(t) = \ell$ for all time and $\lim_{t\to\infty} \alpha(t) = w(2b) - w(0)$. Furthermore, we can explicitly solve for

$$u(x,t) = W(x+b) - W(x-b) + e^{-t}\left[u_0(x) - W(x+b) + W(x-b)\right],$$

so $\lim_{t\to\infty} u(x,t) \equiv U_b(x)$, uniformly on $\mathbb{R}$. We call this case stagnation as the active region remains fixed for $t > 0$ (Fig. 3C).

To summarize, we have shown the following result.

Starting with smooth unimodal even initial conditions, $u_0(x) = u_0(-x)$, with a single active region, $u_0(x) \geq \kappa$ for $|x| \leq \ell$ and $u_0(x) < \kappa$ elsewhere, $\ell > 0$ satisfying $u_0'(x) \gtrless 0$ for $x \lessgtr 0$, the fate of the solutions $u(x,t)$ to the Cauchy problem, Eq (1), falls into three cases:

(i) If $\ell > W^{-1}(\kappa)/2$, then $u \to 1$ locally uniformly on $\mathbb{R}$ as $t \to +\infty$;

(ii) If $\ell < W^{-1}(\kappa)/2$, then $u \to 0$ uniformly on $\mathbb{R}$ as $t \to +\infty$;

(iii) If $\ell = W^{-1}(\kappa)/2$, then $u \to U_b$ uniformly on $\mathbb{R}$ as $t \to +\infty$.

3.2. Interface equations and criticality: asymmetric case. We can extend our analysis to unimodal but asymmetric initial conditions, $u_0(x) \neq u_0(-x)$. Conditions can be stated in terms of the active region of the initial condition $A(0) = [\bar{x}_1, \bar{x}_2]$, where $u_0(x) \geq \kappa$. The active region of $u(x,t)$ is now defined $A(t) = [x_1(t), x_2(t)]$ with associated spatial gradients $\alpha_j(t) = \partial_x u(x_j(t), t)$ for $j = 1, 2$. Carrying out a derivation of the interface dynamics then yields [15, 33]

$$(16a) \qquad x_j'(t) = -\frac{1}{\alpha_j(t)}\left[W(x_2(t) - x_1(t)) - \kappa\right],$$

$$(16b) \qquad \alpha_j(t) = u_0'(x_j(t))e^{-t} + e^{-t}\int_0^t e^s\left[w(x_j(t) - x_1(s)) - w(x_j(t) - x_2(s))\right]\mathrm{d}s,$$

along with initial conditions $x_j(t) = \bar{x}_j$ and $\alpha_j(0) = u_0'(\bar{x}_j)$ for $j = 1, 2$, now requiring $\alpha_1(t) > 0$ and $\alpha_2(t) < 0$. Criticality occurs for initial conditions such that $x_j'(t) = 0$, which means $W(\bar{x}_2 - \bar{x}_1) = \kappa$, so the critical width $2b := W^{-1}(\kappa)$ is precisely the width of the stationary bump $U_b(x)$. Similar to our findings in the symmetric case, we can show: (i) propagation occurs if $\bar{x}_2 - \bar{x}_1 > 2b$; (ii) extinction occurs for $\bar{x}_2 - \bar{x}_1 < 2b$; and (iii) stagnation occurs for $\bar{x}_2 - \bar{x}_1 = 2b$.

3.3. Asymptotic results. As demonstrated, we can predict the long term dynamics of Eq. (1) based on the initial condition $u_0(x)$ and a subsequent analysis of the interface dynamics. The interface equations also allow us to derive convenient asymptotic approximations to the speed of propagating solutions and the time to extinction of decaying solutions. To do so, we truncate the interface system, Eq. (14) and (15), to leading order in the symmetric case.

Long term propagation speed. For propagating solutions, we know $\lim_{t\to\infty} a(t) = +\infty$. Assuming the interface propagates at constant speed $a(t) \sim ct + a_0$ in the limit $t \to \infty$, self-consistency is enforced by plugging into Eq. (15) and evaluating

$$\lim_{t\to\infty} \alpha(t) = \lim_{t\to\infty}\left[u_0'(a(t))e^{-t} + \int_0^t e^{-(t-s)}\left[w(c(t+s) + 2a_0) - w(c(t-s))\right]\mathrm{d}s\right]$$

$$= -\lim_{t\to\infty}\int_0^t e^{-(t-s)}w(c(t-s))\mathrm{d}s = -\frac{1}{c}\int_0^\infty e^{-y/c}w(y)\mathrm{d}y := \bar{\alpha}.$$

8

Differentiating Eq. (9) for $U_f(\xi)$ and plugging in $\xi = 0$, we obtain the same formula, so $\bar{\alpha} = U_f'(0)$, the gradient of the traveling front solution at the threshold κ. Plugging into Eq. (14) along with our assumption $a(t) = ct + a_0$, we find an implicit equation for c, $\int_0^\infty e^{-y/c} w(y) dy = W_\infty - \kappa$, which matches Eq. (10).

Time to extinction. To approximate the extinction time t_0 when $a(t_0) = 0$ in the case $\ell < W^{-1}(\kappa)/2$, we work in the limit $0 < \ell \ll 1$. As $0 < a(t) < \ell$ for time $t \in (0, t_0)$, a Taylor expansion of Eqs. (14) and (15) in $0 < a(t) \ll 1$ implies $\alpha(t)$ and t_0 are small too. In this case, we can approximate $\alpha(t) \approx u_0''(0)\ell$, using the leading order term in Eq. (15), so plugging into Eq. (14) and integrating we can estimate

$$(17) \qquad \frac{\ell}{\kappa} \approx \frac{t_0}{\ell|u_0''(0)|} \quad \Rightarrow \quad t_0 \approx \ell^2 |u_0''(0)|/\kappa \text{ as } \ell \to 0.$$

3.4. Critical stimulus for activation. We now consider the impact of spatiotemporal inputs $I(x,t)$ on the long term dynamics of Eq. (1) when $u_0(x) \equiv 0$. This may be more biologically realistic than assuming arbitrary initial conditions, as waves are often initiated experimentally in cortical tissue by applying an external stimulus [16, 23, 44]. To provide intuition, we first construct stationary solutions assuming $I(x,t) \equiv I(x)$ is unimodal ($I'(0) = 0$ and $I'(x) \gtrless 0$ for $x \lessgtr 0$), positive $I(x) > 0$, and even $I(x) = I(-x)$. When $\max_{x \in \mathbb{R}} I(x) = I(0) > \kappa$, we show that if there are any stationary bump solutions, the one with minimal half-width $b_{\min}$ is linearly stable. Subsequently, we derive conditions for a brief stimulus lasting a time t_1, $I(x,t) = I(x)\chi_{[0,t_1]}$ ($\chi_{[0,t_1]} = 1$, $t \in [0, t_1]$; 0 otherwise), that ensure propagation of solutions for times $t > t_1$. We show that: (i) there must be no stationary bump solutions to Eq. (1) with $I(x,t) = I(x)$; and (ii) the active region at $t = t_1$ must be wider than that of the critical bump $U_b(x)$ of the input-free system.

Stationary bump solutions to Eq. (1) for $I(x,t) \equiv I(x)$ with a single active region have the form $U_b(x) = W(x+b) - W(x-b) + I(x)$. The threshold condition

$$(18) \qquad U_b(\pm b) = W(2b) + I(b) = G(b) = \kappa$$

defines an implicit equation for the half-width b. An algebraic argument can be used to show that if there are solutions b to Eq. (18), they will all be less than the solution to the input-free case $I \equiv 0$: $b < b_0 = W^{-1}(\kappa)/2$. See Fig. 4A for illustration. Local analysis can be used to show that the sign of $G(b)$ determines the stability of a bump of half-width b ($G(b) < 0$: stable; $G(b) > 0$: unstable), and if there are any solutions to Eq. (18), the minimal one $b_{\min}$ will be stable or marginally stable [24].

We now demonstrate that for a spatiotemporal input, $I(x,t) = I(x)\chi_{[0,t_1]}$, to generate propagation, (i) Eq. (18) must have no solutions, and (ii) t_1 must be large enough so the active region $A(t) = [-a(t), a(t)]$ satisfies $a(t_1) > b_0$, where b_0 solves Eq. (18) for $I \equiv 0$. Starting from $u_0(x) \equiv 0$, we know initially, the dynamics obeys $\partial_t u(x,t) = -u(x,t) + I(x,t)$, so $u(x,t) = I(x)(1 - e^{-t})$ during this phase. This formula determines the lower bound on the stimulus time $t_0 < t_1$ needed to generate a nontrivial active region, $A(t) \neq \emptyset$. This time is given by solving

$$\max_{x \in \mathbb{R}} u(x, t_0) = I(0)(1 - e^{-t_0}) = \kappa \quad \Rightarrow \quad t_0 = \ln\left[\frac{I(0)}{I(0) - \kappa}\right].$$

If $t_1 \leq t_0$, then the long term dynamics of the solution is $u(x,t) = I(x)(1 - e^{-t_1})e^{-(t-t_1)}$ for $t > t_1$, and $\lim_{t \to \infty} u(x,t) \equiv 0$. Note if $I(0) < \kappa$, then $u(x,t) < \kappa$ for all $t > 0$.
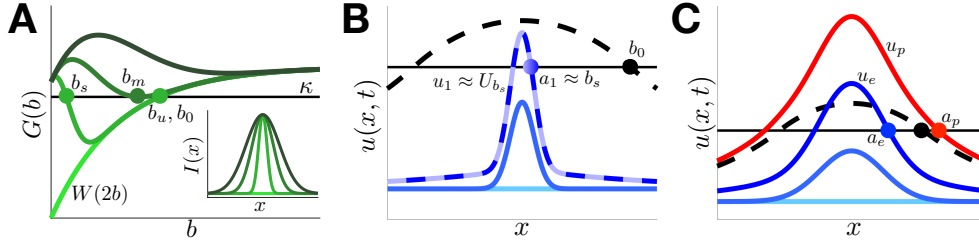
FIG. 4. *Conditions for propagation driven by the input $I(x,t) = I(x)\chi_{[0,t_1]}$, when $u(x,0) \equiv 0$. (A) For symmetric, unimodal, and positive profile $I(x)$ with $I(0) > \kappa$, propagation will only occur if $G(b) = W(2b) + I(b) = \kappa$ has no solutions, which occurs for sufficiently wide $I(x)$ (note inset). If solutions to Eq. (18) exist, the minimal one will be linearly (b_s) or marginally (b_m) stable. Corresponding unstable solutions b_u will typically be close to b_0, the solution to $W(2b_0) = \kappa$. (B) For $I(x)$ such that $G(b_s) = \kappa$ for some b_s, $u(x,t_1) \approx U_{b_s}(x)$ for large enough t_1 with active region $[-a_1, a_1]$ for $a_1 := a(t_1) < b_0$, so $\lim_{t\to\infty} u(x,t) \equiv 0$. (C) Here, $I(x)$ is chosen such that $G(b) = \kappa$ has no solutions. Taking t_e such that $u_e = u(x,t_e)$ satisfies $u(\pm a_e, t_e) = \kappa$ with $a_e < b_0$, then $\lim_{t\to\infty} u(x,t) \equiv 0$. On the other hand, for t_p such that $u_p = u(x,t_p)$ satisfies $u(\pm a_p, t_p) = \kappa$ with $a_p > b_0$, then $u(x,t)$ propagates as $t \to \infty$.*

If $t_1 > t_0$, then for $t_0 < t < t_1$, we can derive the interface equations for $u(\pm a(t), t) = \kappa$, which are

$$(19a) \qquad a'(t) = -\frac{1}{\alpha(t)} \left[W(2a(t)) - \kappa + I(a(t)) \right],$$

$$(19b) \qquad \alpha(t) = e^{-t} \int_{t_0}^{t} e^{s} \left[w(a(t) + a(s)) - w(a(t) - a(s)) + I'(a(s)) \right] ds,$$

with initial conditions $a(t_0) = 0$ and $\alpha(t_0) = 0$, so $a'(t_0)$ diverges. Despite the singularity, we can show that $a'(t)$ is integrable for $|t - t_0| \ll 1$ and $a(t), \alpha(t) \propto \sqrt{t - t_0}$. We desingularize Eq. (19) with the change of variables $\tau = -\int_{t_0}^{t} \frac{ds}{\alpha(s)}$ [3, 4], so the differential equation for $\tilde{a}(\tau)$ in the new coordinate frame is

$$(20) \qquad \frac{d\tilde{a}}{d\tau}(\tau) = W(2\tilde{a}(\tau)) - \kappa + I(\tilde{a}(\tau)),$$

with $\tilde{a}(0) = 0$. Since we know $\alpha(t) < 0$ for $t > t_0$, then τ will be an increasing function of t, so we refer now to $\tau_1 := \tau(t_1)$ and note $0 = \tau(t_0)$. Because $I(0) - \kappa > 0$ by assumption, we have $\frac{d\tilde{a}}{d\tau}(\tau) > 0$ for all τ where it is defined.

There are three remaining cases now, which depend on the existence of solutions to Eq. (18) and the time $\tau_1 > 0$: (I) Eq. (18) has at least one solution, and propagation does not occur; (II) Eq. (18) has no solutions, but $\tau_1 \leq \tau_c$, the time at which $\tilde{a}(\tau_c) = b_0$ for $I(x, \tau) \equiv I(x)$, and propagation does not occur; (III) Eq. (18) has no solutions, and $\tau_1 > \tau_c$, so propagation occurs. We now treat these three cases in detail.

Case I: $\min_{x \in \mathbb{R}} G(x) \leq \kappa$. Here, Eq. (18) possesses at least one solution. By our assumption $I(0) > \kappa$, this solution $b_{\min}$ is linearly or marginally stable, as mentioned. Eq. (20) implies $\frac{d\tilde{a}}{d\tau} > 0$ for all $\tau < \tau_1$, but $\frac{d\tilde{a}}{d\tau}$ vanishes at $\tilde{a} = b_{\min}$, so $\tilde{a}(\tau) < b_{\min} < b_0$ for all $\tau < \tau_1$. Thus, once $\tau = \tau_1$, the dynamics is described by the extinction case detailed in Section 3.1, and $\lim_{t\to\infty} u(x,t) \equiv 0$ (Fig. 4B).

Case II: $\min_{x \in \mathbb{R}} G(x) > \kappa$ *and* $\tau_1 \leq \tau_c$. Here Eq. (18) has no solutions, but $\tilde{a}(\tau)$ will not grow large enough for propagation to occur once the input $I(x, \tau)$ is terminated. This is due to the condition $\tau_1 \leq \tau_c$, where we can define the critical time τ_c as the

10

time when $\tilde{a}(\tau_c) = b_0 = W^{-1}(\kappa)/2$ as

$$(21) \qquad \int_0^{W^{-1}(\kappa)/2} \frac{\mathrm{d}a}{W(2a) - \kappa + I(a)} = -\int_{t_0}^{t_c} \frac{\mathrm{d}t}{\alpha(t)} := \tau_c.$$

By definition $\tilde{a}(\tau_1) \leq b_0$, so once $\tau = \tau_1$, the dynamics is described by (a) the extinction case in Section 3.1 if $\tau_1 < \tau_c$, so $\lim_{t\to\infty} u(x,t) \equiv 0$, or (b) the stagnation case in Section 3.1 if $\tau_1 = \tau_c$, so $\lim_{t\to\infty} u(x,t) \equiv U_b(x)$ (Fig. 4C).

Case III: $\min_{x\in\mathbb{R}} G(x) > \kappa$ *and* $\tau_1 > \tau_c$. Finally, we describe the case ensuring propagation for $t \to \infty$. Requiring $\tau_1 > \tau_c$ with Eq. (21), we have that $\tilde{a}(\tau_1) > b_0$. After $\tau = \tau_1$, the dynamics is described by the propagation case in Section 3.1, so the homogeneous state $u \equiv 1$ is locally uniformly propagating as $t \to \infty$ (Fig. 4C).

3.5. Explicit results for exponential kernel. Lastly, we demonstrate the results derived above using the exponential kernel, Eq. (2). The form of the interface equations for symmetric initial conditions and $I \equiv 0$ are

$$(22a) \qquad a'(t) = -\frac{1}{2\alpha(t)} \left[1 - \mathrm{e}^{-2a(t)} - 2\kappa \right],$$

$$(22b) \qquad \alpha(t) = u_0'(a(t))\mathrm{e}^{-t} - \mathrm{e}^{-t-a(t)} \int_0^t \mathrm{e}^s \sinh(a(s))\mathrm{d}s.$$

First, note the critical half-width b_0 is given by when $a'(t) = 0$, which here is $b_0 = -\frac{1}{2} \ln [1 - 2\kappa]$, so if $a(0) > b_0$, propagation occurs. We demonstrate the accuracy of this boundary in predicting long-term dynamics by comparing with numerically computed boundaries in Fig. 5A. Note, in the case of propagation, in the limit $t \gg 1$, we can approximate $a(t) \approx ct + a_0$, and the asymptotic approximation in Section 3.3 yields $\frac{c}{2(c+1)} = \frac{1}{2} - \kappa$, which we rearrange to yield [6,19,36]

$$c = \frac{1}{2\kappa} [1 - 2\kappa], \qquad \bar{\alpha} = -\frac{2\kappa}{1 - 2\kappa} \cdot \frac{1 - 2\kappa}{2} = -\kappa.$$

To quantify the timescale of approach to the asymptotic dynamics, we study the evolution of perturbations to the long term wavespeed c, $a(t) = ct + a_0 + \phi(t)$ and assuming $\alpha(t) \approx -\kappa$. Plugging into Eq. (22), and truncating assuming $\phi(t)$ and e^{-2a_0} are of similar order, we find

$$2\kappa\phi'(t) = \mathrm{e}^{-2(ct+a_0)} \quad \Rightarrow \quad \phi(t) = -\frac{\mathrm{e}^{-2a_0}}{4\kappa c}\mathrm{e}^{-2ct},$$

and $a(t)$ approaches the propagation speed c at rate $2c$. We compare this result to our findings from numerical simulations in Fig. 5B. We save a higher order asymptotic analysis for future work. In addition, we can compute the asymptotic extinction time for the case in which $u_0(x) = \mathcal{U}\mathrm{e}^{-x^2/(2\sigma^2)}$, so $|u_0''(0)| = \mathcal{U}/\sigma^2$ and $\kappa = u_0(\ell)$ implies

$$\ell = \sigma\sqrt{2}\sqrt{\ln(\mathcal{U}/\kappa)} \quad \Rightarrow \quad t_0 \approx \ell^2 \mathrm{e}^{\ell^2/(2\sigma^2)}/\sigma^2,$$

which agrees with numerical simulations for small enough ℓ (Fig. 5C).

The critical stimulus for activation was determined in for a general weight kernel in Section 3.4. Note, the main conditions are that Eq. (18) has no solutions, and that the stimulus remains on for a time $t > t_c$, where t_c is defined by the relation in Eq. (21).
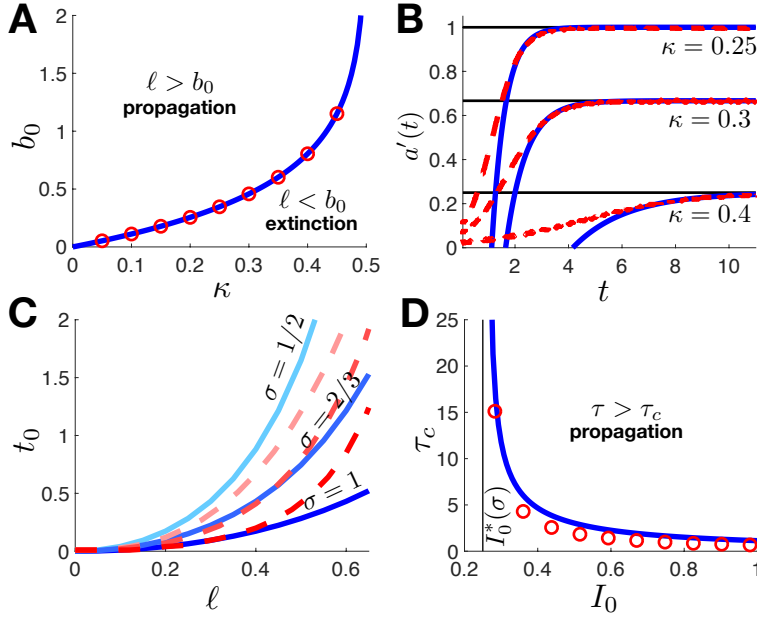
11

FIG. 5. *Bounds and asymptotics for an exponential kernel, $w(x) = e^{-|x|}/2$. (A) Propagation occurs if $\ell := a(0) > b_0$ for $b_0 = -\ln[1 - 2\kappa]/2$ (solid line); extinction occurs if $\ell < b_0$. Numerical simulations (circles) determine b_0 by computing Eq. (1) starting with $u(x, 0) = u_0(x)$ and identifying b_0 for which stagnation occurs ($u_0(b_0) = \kappa$). Results are consistent whether choosing $u_0(x) = \mathcal{U} \cdot U_b(x), \mathcal{U}e^{-x^2}$, or $\left[\mathcal{U}(1 - x^2)\right]_+$. (B) Instantaneous speed of interface $a'(t) \to c(\kappa)$ in numerical simulations (dashed lines). For $a'(t) \approx c$, the approach is well characterized by the asymptotic estimate $a'(t) \approx c - c_1 e^{-2ct}$ (solid line) for best fit c_1. (C) Extinction time $t_0 \approx \ell e^{\ell^2/(2\sigma^2)}/\sigma^2$ (solid line) estimated for $u_0(x) = \mathcal{U}e^{-x^2/(2\sigma^2)}$ compared with numerical simulations. (D) Critical time τ_c (in rescaled coordinate $\tau = -\int_{t_0}^t \frac{ds}{\alpha(s)}$) the input $\tilde{I}(x, \tau) = I_0\chi_{[0,\tau_1]}e^{-5|x|}$ must be on for propagation to occur, computed from Eq. (21) by integrating in a using quadrature (solid line) or computing Eq. (1) and numerically computing the integral in t (circles). As $I_0 \to I_0^*(\sigma)$, the minimal τ for propagation, τ_c, blows up.*

For an exponential weight kernel, Eq. (2) and exponential input $I(x) = I_0 e^{-|x|/\sigma}$ (See also [24]), Eq. (18) becomes $\kappa = (1 - e^{-2b})/2 + I_0 e^{-b/\sigma} = G(b)$, so

$$G'(b) = e^{-2b} - \frac{I_0}{\sigma}e^{-b/\sigma} = 0 \quad \Rightarrow \quad b^* = \sigma \ln[I_0/\sigma]/(1 - 2\sigma)$$

and also $\lim_{b \to 0^+} G'(b) = 1 - I_0/\sigma$. Therefore if the input is sufficiently wide, $\kappa < I_0 < \sigma$ and $1/2 < \sigma$, then initially $G(b)$ increases until $b^* > 0$, and then it decreases to $1/2$ for large b, so $G(b) > \kappa$ for all $b > 0$ for sufficiently wide inputs with $I_0 > \kappa$. In addition, even for $I_0 > \sigma > 1/2$, then $b^* < 0$, and since we know $\lim_{b \to \infty} G(b) = 1/2$, then $G(b) > 1/2$ since it must be monotone decreasing for all $b > 0$. Thus, there are no stable bump solutions to Eq. (18) for sufficiently wide and strong inputs. On the other hand, if we wish to determine the critical curve $I_0^*(\sigma)$ below which bump solutions to Eq. (18) emerge (assuming $I_0 > \kappa$), we simultaneously solve $G(b) = \kappa$ and $G'(b) = 0$ to find the saddle-node bifurcation point

$$I_0^*(\sigma) = \sigma \frac{1 - 2\sigma}{1 - 2\kappa} e^{(1-2\sigma)/(2\sigma)}.$$

Taking $I_0 \leq I_0^*(\sigma)$ then ensures the existence of bumps (as in Fig. 4A). For $I_0 > I_0^*(\sigma)$, we can also study the impact of the input on the time necessary to reach $a(t) = b_0$,

using the integral over a in Eq. (21). We evaluate this numerically in Fig. 5D, showing it compares well with estimates we obtain by computing the critical time t_c numerically and then converting to τ coordinates using the change of variables in Eq. (21). Note that as $I_0 \to I_0^*(\sigma)$, then $\tau_c \to \infty$.

4. Multiple active regions. We now turn our attention to the more general case of multimodal initial conditions. Since this can now lead to multiple disjoint active regions (where $u_0(x) \geq \kappa$), we must extend our analysis from Section 3 to track more than two interfaces (See also [33]). While it is difficult to analyze the resulting system of equations explicitly, we can gain insight by focusing on two specific cases of $u_0(x)$: (a) periodic initial conditions with an infinite number of active regions and (b) two symmetric active regions. We begin by deriving the interface equations in the general case.

4.1. Interface equations: general case. When $u_0(x) \geq \kappa$ for multiple disjoint active regions, $A(0) = \cup_{j=1}^{N} [a_j(0), b_j(0)]$, the time evolution of $A(t)$ is implicitly described by

$$(23) \qquad u(a_j(t), t) = u(b_j(t), t) = \kappa, \qquad j = 1, ..., N,$$

for an initial time $0 < t < t_0$. Differentiating Eq. (23) with respect to t, we find

$$(24) \quad \alpha_j(t) a_j'(t) + \partial_t u(a_j(t), t) = 0, \quad \beta_j(t) b_j'(t) + \partial_t u(b_j(t), t) = 0, \quad j = 1, ..., N,$$

where $\alpha_j(t) = \partial_x u(a_j(t), t)$ and $\beta_j(t) = \partial_x u(b_j(t), t)$. Rearranging Eq. (24), applying Eq. (11) for u_t, and solving for $z = u_x$ as before, we find the following system describing the evolution of the interfaces $(a_j(t), b_j(t))$ and gradients $(\alpha_j(t), \beta_j(t))$:

$$(25a) \quad a_j'(t) = -\frac{1}{\alpha_j(t)} \left[\sum_{k=1}^{N} \left(W(b_k(t) - a_j(t)) - W(a_k(t) - a_j(t)) \right) - \kappa \right],$$

$$(25b) \quad b_j'(t) = -\frac{1}{\beta_j(t)} \left[\sum_{k=1}^{N} \left(W(b_k(t) - b_j(t)) - W(a_k(t) - b_j(t)) \right) - \kappa \right],$$

$$(25c) \quad \alpha_j(t) = e^{-t} \int_0^t e^s \sum_{k=1}^{N} \left[w(a_j(t) - a_k(s)) - w(a_j(t) - b_k(s)) \right] ds + u_0'(a_j(t)) e^{-t},$$

$$(25d) \quad \beta_j(t) = e^{-t} \int_0^t e^s \sum_{k=1}^{N} \left[w(b_j(t) - a_k(s)) - w(b_j(t) - b_k(s)) \right] ds + u_0'(b_j(t)) e^{-t},$$

for $j = 1, ..., N$. The initial conditions $u_0(a_j(0)) = u_0(b_j(0)) = \kappa$ close the system. We expect $\alpha_j(t) \geq 0$ and $\beta_j(t) \leq 0$, since they are at the left and right boundaries of each active region. For the system Eq. (25), there is no straightforward condition that will ensure propagation in all cases (e.g., see Fig. 1C). For $N = 1$, Eq. (25) reduces to Eq. (16), and recall we can explicitly compute the condition for propagation.

First note that one could solve Eq. (25) much faster numerically than Eq. (1), allowing a computational route to identifying conditions on $u_0(x)$ that determine propagation. We save such computations for future work. Here, we focus on two special choices of initial conditions that admit explicit analysis: initial conditions that are (a) periodic and (b) even symmetric with two active regions.
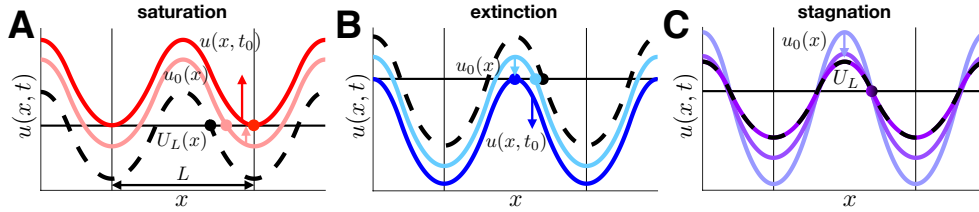
13

FIG. 6. *Long term behavior of $u(x,t)$, given a periodic initial condition with $u_L(\pm\ell_L + nL) = \kappa$, $\forall n \in \mathbb{Z}$, depends on relation between ℓ_L and $b_L = \mathbf{W}_L^{-1}(\kappa)$. (A) If $\ell_L > b_L$, saturation occurs, and $\lim_{t\to\infty} u(x,t) \equiv 1$. (B) If $\ell_L < b_L$, extinction occurs, and $\lim_{t\to\infty} u(x,t) \equiv 0$. (C) If $\ell_L = b_L$, stagnation occurs, and $\lim_{t\to\infty} u(x,t) = U_L(x)$ as in Eq. (5).*

4.2. Periodic initial conditions. We can leverage results on periodic stationary solutions derived in Section 2.2 along with the analysis for single active regions in Section 3.1 to derive conditions for saturation $(u \to 1)$ when initial conditions are periodic. For an even and periodic initial condition $u(x,0) = u_L(x)$ of period L, $A(t) = \cup_{n\in\mathbb{Z}} [-a(t) + nL, a(t) + nL]$, so by symmetry we can reduce Eq. (25) to

$$(26a) \qquad a'(t) = -\frac{1}{\alpha(t)} \left[\mathbf{W}_L(a(t)) - \kappa \right],$$

$$(26b) \qquad \alpha(t) = u_L'(a(t))\mathrm{e}^{-t} + \mathrm{e}^{-t} \int_0^t \mathrm{e}^s \sum_{n\in\mathbb{Z}} w_n(a(t), a(s))\mathrm{d}s,$$

where $w_n(a(t), a(s)) = w(a(t) + a(s) + nL) - w(a(t) - a(s) + nL)$ and $\mathbf{W}_L(x)$ is defined as in Eq. (6). Fixing L, the initial condition $u_L(x)$ is defined by the single parameter $\ell_L := a(0)$, where $u_L(\pm\ell_L + nL) = \kappa$, $\forall n \in \mathbb{Z}$. Criticality occurs for $\ell_L = b_L(\kappa) = \mathbf{W}_L^{-1}(\kappa)$, the half-width of each active region of the periodic solution $U_L(x)$, Eq. (5). The analysis proceeds along similar lines to that given in Section 3.1 for the single active region case yielding the following results (illustrated in Fig. 6):

Starting with smooth L-periodic, even initial conditions, $u_L(x)$, unimodal on $[-L/2, L/2]$, the fate of the solutions $u(x,t)$ to Eq (1), falls into three cases:

(i) *If $\ell_L > \mathbf{W}_L^{-1}(\kappa)$, then $u \to 1$ uniformly on $\mathbb{R}$ as $t \to +\infty$;*

(ii) *If $\ell_L < \mathbf{W}_L^{-1}(\kappa)$, then $u \to 0$ uniformly on $\mathbb{R}$ as $t \to +\infty$;*

(iii) *If $\ell = \mathbf{W}_L^{-1}(\kappa)$, then $u \to U_L$ uniformly on $\mathbb{R}$ as $t \to +\infty$.*

Asymptotic results. Similar to the single active region case, we can obtain leading order approximations for the transient dynamics approaching the homogeneous states. For periodic initial conditions, we do not obtain traveling waves in the long time limit. In the case of saturation, we can estimate the time t_0 at which $u(x,t_0) \geq \kappa$, assuming $L/2 - a(t)$, $\alpha(t)$, and t_0 are small. We approximate $\alpha(t) \approx u_L''(L/2)(\ell_L - L/2)$, so $t_0 \approx (L - 2\ell_L)^2 u_L''(L/2)/[2 - 4\kappa]$.

In the case of extinction, the calculation is quite similar to that presented in Section 3.3, and we find $u(x,t_0) \leq \kappa$ at $t_0 \approx \ell_L^2 |u_L''(0)|/\kappa$ in the limit $0 < \ell_L \ll 1$.

Exponential kernels. Assuming $w(x)$ is given by Eq. (2), we can obtain a simple implicit expression for the critical half-width $b_L := \mathbf{W}_L^{-1}(\kappa)$. Plugging Eq. (2) into Eq. (6), we can simplify the threshold condition $U_L(\pm b + nL) = \kappa$ to the form [32]

$$(27) \qquad \kappa = \frac{\sinh(b)}{\sinh(L/2)} \cosh(L/2 - b) := \mathbf{W}_L(b).$$

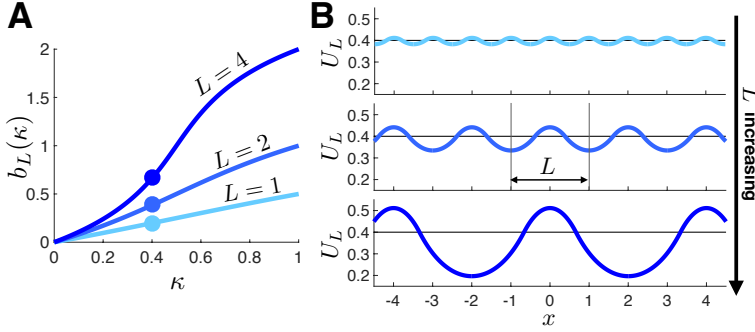Eq. (27) must be solved numerically (Fig. 7A), showing b_L increases with κ and L.

FIG. 7. *Stationary periodic solutions U_L to Eq. (1) with exponential kernel, Eq. (2). (A) Half-width b_L of the active region on each period L increases with threshold κ and period L, as determined by Eq. (27). (B) Increasing L yields periodic patterns (corresponding to dots in panel A at $\kappa = 0.4$) with wider active regions and higher amplitude oscillations, as determined by Eq. (28).*

The formula for U_L can also be reduced to yield

$$
(28) \qquad U_L(x) = \begin{cases} \dfrac{\sinh(b)}{\sinh(L/2)} \cosh\left(\dfrac{L}{2} + x_n\right), & x_n \in (b - L, -b), \\[2mm] 1 - \dfrac{\mathrm{e}^{L-b} - \mathrm{e}^b}{\mathrm{e}^L - 1} \cosh(x_n), & x_n \in (-b, b), \\[2mm] \dfrac{\sinh(b)}{\sinh(L/2)} \cosh\left(\dfrac{L}{2} - x_n\right), & x_n \in (b, L - b), \end{cases}
$$

where we define $x_n := x - nL$, $\forall n \in \mathbb{Z}$ (Fig. 7B). Note, we obtain the threshold condition, Eq. (27) for $U_L(\pm b + nL)$, $\forall n \in \mathbb{Z}$, and as $L \to \infty$, $U_L(x) \to U_b(x)$.

4.3. Two symmetric active regions. We now consider the case of of bi-modal even initial conditions $u_0(x) = u_0(-x)$, with two active regions supported in $[-\ell_2, -\ell_1] \cup [\ell_1, \ell_2]$ for $0 < \ell_1 < \ell_2$. That is, we have $u_0(x) \geq \kappa$ for all $x \in [-\ell_2, -\ell_1] \cup [\ell_1, \ell_2]$ and $u_0(x) < \kappa$ elsewhere, with $u_0'(x) \gtrless 0$ for $x \lessgtr \mp \ell_2$. We also ensure a non-degeneracy condition of the derivative of u_0 at the boundaries of the active regions, namely $u_0'(\pm \ell_{1,2}) \neq 0$. These hypotheses on the initial conditions ensure that, as time evolves, the active regions can be described by the inner inter-face $a(t) := a_2(t) = -b_1(t)$, outer interface $b(t) := b_2(t) = -a_1(t)$, outer gradient $\alpha(t) := \alpha_2(t) = -\beta_1(t)$, and inner gradient $\beta(t) := \beta_2(t) = -\alpha_1(t)$. We can therefore write the system of interface equations and their gradients, Eq. (25), in the following simpler form

$$
(29a) \qquad a'(t) = -\frac{1}{\alpha(t)} \left[W(b(t) - a(t)) - \kappa + W(b(t) + a(t)) - W(2a(t)) \right],
$$

$$
(29b) \qquad b'(t) = -\frac{1}{\beta(t)} \left[W(b(t) - a(t)) - \kappa + W(2b(t)) - W(b(t) + a(t)) \right],
$$

$$
\alpha(t) = u_0'(a(t))\mathrm{e}^{-t} + \mathrm{e}^{-t} \int_0^t \mathrm{e}^s \left[w(a(t) + b(s)) - w(a(t) + a(s)) \right] \mathrm{d}s,
$$

$$
(29c) \qquad\qquad + \mathrm{e}^{-t} \int_0^t \mathrm{e}^s \left[w(a(t) - a(s)) - w(a(t) - b(s)) \right] \mathrm{d}s,
$$

$$
\beta(t) = u_0'(b(t))\mathrm{e}^{-t} + \mathrm{e}^{-t} \int_0^t \mathrm{e}^s \left[w(b(t) - a(s)) - w(b(t) - b(s)) \right] \mathrm{d}s
$$

15

$$(29d) \qquad\qquad + e^{-t} \int_0^t e^s \left[w(b(t) + b(s)) - w(b(t) + a(s)) \right] ds.$$

The system Eq. (29) is closed by the initial conditions $a(0) = \ell_1$ and $b(0) = \ell_2$. As opposed to the single active region case, it is not possible to develop a simple condition on (ℓ_1, ℓ_2) that determines whether propagation, extinction, or stagnation occurs in the long time limit. However, we can still partition the space of initial conditions (ℓ_1, ℓ_2) into several cases, for which the long term behavior of Eq. (1) is determined by the initial transient dynamics of $(a(t), b(t))$. Observe that both $W(b(t)+a(t))-W(2a(t)) > 0$ and $W(2b(t))-W(b(t)+a(t)) > 0$ for all time whenever they are well defined (*i.e.* as long as $0 < a(t) < b(t)$). As a consequence, we can already rule out the trivial case where $\ell_2 - \ell_1 \geq W^{-1}(\kappa)$.

Class I: $\ell_2 - \ell_1 \geq W^{-1}(\kappa)$. In this case, we automatically deduce that $b'(t) > 0$ while $a'(t) < 0$ for all time where they are both well defined. This implies that there exists a finite $t_* > 0$ at which we have $a(t_*) = 0$. At this point, the two active regions merge to form a single active region given at time $t = t_*$ by $[-b(t_*), b(t_*)]$ with $2b(t_*) > 2\ell_2 > W^{-1}(\kappa)$ as $\ell_2 - \ell_1 \geq W^{-1}(\kappa)$. As a consequence, we are back to the propagation scenario studied in Section 3.1 and we find the associated solution of the neural field Eq. (1) obeys $u \to 1$ locally uniformly on $x \in \mathbb{R}$ as $t \to +\infty$.

Class II: $\ell_2 - \ell_1 < W^{-1}(\kappa)$. We now discuss the case where $\ell_2 - \ell_1 < W^{-1}(\kappa)$. In order to simplify the presentation, we define the following two quantities:

$$\mathcal{W}_1(\ell_1, \ell_2) := W(\ell_2 - \ell_1) - \kappa + W(\ell_1 + \ell_2) - W(2\ell_1),$$
$$\mathcal{W}_2(\ell_1, \ell_2) := W(\ell_2 - \ell_1) - \kappa + W(2\ell_2) - W(\ell_1 + \ell_2),$$

defined for all $0 < \ell_1 < \ell_2$. It is crucial to observe that $\mathcal{W}_1(\ell_1, \ell_2) - \mathcal{W}_2(\ell_1, \ell_2) = 2W(\ell_1 + \ell_2) - W(2\ell_1) - W(2\ell_2) > 0$ for any $0 < \ell_1 < \ell_2$ by concavity of the function W on the positive half line. Thus, we only have to consider three cases (See Fig. 8).

Case A: If $\mathcal{W}_1(\ell_1, \ell_2) > \mathcal{W}_2(\ell_1, \ell_2) \geq 0$, then $b'(t) > 0$ and $a'(t) < 0$ for all time where they are both well defined. Once again, there must exist $t_* > 0$ at which $a(t_*) = 0$. At that point, the two active regions merge to form a single active region given at time $t = t_*$ by $[-b(t_*), b(t_*)]$ with $2b(t_*) > 2\ell_2 > W^{-1}(\kappa)$. Indeed, from $\mathcal{W}_2(\ell_1, \ell_2) > 0$, we deduce that $W(2\ell_2) > W(\ell_1 + \ell_2) - W(\ell_2 - \ell_1) + \kappa > \kappa$. And we are back to the propagation case of Section 3.1.

Case B: If $0 \geq \mathcal{W}_1(\ell_1, \ell_2) > \mathcal{W}_2(\ell_1, \ell_2)$, then $b'(t) < 0$ and $a'(t) > 0$ for all time where they are both well defined. As a consequence, there exists some time $t_* > 0$ where $a(t_*) = b(t_*)$ and such that $u(x, t_*) \leq \kappa$ for all $x \in \mathbb{R}$. As a consequence, this will lead to the extinction case of Section 3.1 and we get that the solutions of the neural field equation Eq. (1) obeys $u \to 0$ uniformly on $\mathbb{R}$ as $t \to +\infty$.

Case C: If $\mathcal{W}_1(\ell_1, \ell_2) > 0 > \mathcal{W}_2(\ell_1, \ell_2)$, then we are led to study three sub-cases:

Sub-case 1: Both $a(t)$ and $b(t)$ satisfy $\mathcal{W}_1(a(t), b(t)) > 0 > \mathcal{W}_2(a(t), b(t))$ for all $t \in [0, t_*)$ where they are well defined, and at time $t = t_*$ we have $a(t_*) = 0$. Once more, at this point, the two active regions merge to form a single active region at time $t = t_*$: $[-b(t_*), b(t_*)]$ with $2b(t_*) < 2\ell_2$. Thus, it is enough to check that the limit $t \to t_*$, we have $\mathcal{W}_2(a(t), b(t)) \to W(2b(t_*)) - \kappa$. Since $\mathcal{W}_2$ does not change sign in $(0, t_*)$, then $0 \geq W(2b(t_*)) - \kappa$, so we obtain either stagnation (when $W(2b(t_*)) = \kappa$) or extinction (when $W(2b(t_*)) < \kappa$), as studied in Section 3.1.

Sub-case 2: There exists a time $t_0 > 0$ where $a(t)$ and $b(t)$ satisfy $\mathcal{W}_1(a(t), b(t)) > 0 > \mathcal{W}_2(a(t), b(t))$ for all $t \in [0, t_0)$, and at $t = t_0$ we have $a(t_0) \neq 0$ with $\mathcal{W}_2(a(t_0), b(t_0)) = 0$ while $\mathcal{W}_1(a(t_0), b(t_0)) > 0$, in which case we are back to Case A and propagation occurs.
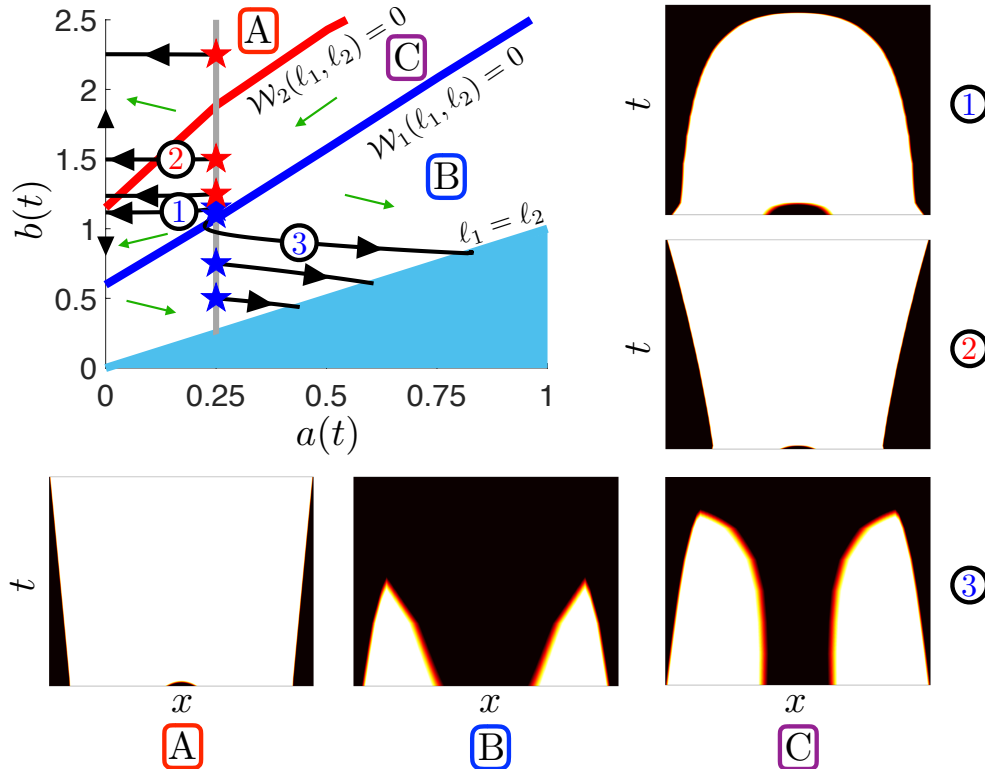
FIG. 8. *Evolution of interfaces for two symmetric bumps having Class II initial conditions: $\ell_2 - \ell_1 < W^{-1}(\kappa)$. Phase portrait of Eq. (29) in $(a(t),b(t))$ is shown in the case of an exponential kernel, Eq. (2), $\kappa = 0.45$ and the initial condition $u_0(x)$, Eq. 30. We fix $a(0) = \ell_1 = 1/4$ and vary $b(0) = \ell_2$ from 0.5 to 2.25. Some initial conditions (red stars) lead to trajectories (black lines) that propagate, while other initial conditions (blue stars) lead to extinction. Case A ($\mathcal{W}_1(\ell_1,\ell_2) > \mathcal{W}_2(\ell_1,\ell_2) \geq 0$): $a(t)$ vanishes in finite time with a final value above the nullcline $\mathcal{W}_2(\ell_1,\ell_2) = 0$ (where red line meets ℓ_2 axis), leading to propagation. See corresponding example evolution of $u(x,t)$. Case B ($0 \geq \mathcal{W}_1(\ell_1,\ell_2) > \mathcal{W}_2(\ell_1,\ell_2)$): $a(t)$ and $b(t)$ merge in finite time, leading to extinction. Case C ($\mathcal{W}_1(\ell_1,\ell_2) > 0 > \mathcal{W}_2(\ell_1,\ell_2)$): Three subcases are described in main text, leading to either extinction for subcases (1) and (3) or propagation for subcase (2). Green arrows indicate the direction of the vector field in each sub-region. Outer panels demonstrate behavior of the full neural field model, Eq. (1), in the cases A, B, C1, C2, and C3.*

Sub-case 3: There exists a time $t_1 > 0$ where $a(t)$ and $b(t)$ satisfy $\mathcal{W}_1(a(t), b(t)) > 0 > \mathcal{W}_2(a(t), b(t))$ for all $t \in [0, t_1)$, and at $t = t_1$ we have $a(t_1) \neq 0$ with $\mathcal{W}_1(a(t_1), b(t_1)) = 0$ while $0 > \mathcal{W}_2(a(t_1), b(t_1))$, in that case we are back to Case B and extinction occurs.

We illustrate these different scenarios on a specific example in Fig. 8 using an exponential kernel, Eq. (2), and the following initial condition

$$
(30) \qquad u_0(x) = \frac{U_0}{2}\left(e^{-|x+x_0|} + e^{-|x-x_0|}\right),
$$

which allows us to specify

$$
x_0 = \frac{1}{2}\ln\left(-1 + 2\cosh(\ell_1)e^{\ell_2}\right), \text{ and } U_0 = \kappa\frac{\sqrt{-1 + 2\cosh(\ell_1)e^{\ell_2}}}{\cosh(\ell_1)},
$$

and ensure that $u_0(\pm\ell_{1,2}) = \kappa$. Note, for a fixed ℓ_1, there is a critical value of ℓ_2 at which initial conditions transition from those that lead to extinction (blue stars)

17

to those that lead to propagation (red stars) in Fig. 8. Corresponding example simulations of the full neural field Eq. (1) are also shown.

4.4. Critical spatially-periodic stimuli. Finally, we can consider the impact of spatially periodic inputs $I(x,t) = I(x)\chi_{[0,t_1]}$ ($I(x) = I(x+L)$) on the long-term dynamics of Eq. (1), assuming $u_0(x) \equiv 0$. To make our calculations more straightforward, we assume that $I(x)$ is even and unimodal on $x \in [-L/2, L/2]$ with $I'(0) = I'(\pm L/2) = 0$. Our analysis follows similar principles as that performed for unimodal inputs in Section 3.4. To ensure propagation, there must be no stationary L-periodic pattern solutions to Eq. (1) with stationary input $I(x)$ and the active region on $x \in [-L/2, L/2]$ at $t = t_1$ must be wider than $b_L = \mathbf{W}_L^{-1}(\kappa)$.

Stationary periodic patterns exist as solutions to Eq. (1) for $I(x,t) = I(x)$ periodic ($I(x) = I(x+L)$), even, and unimodal on $x \in [-L/2, L/2]$. Adapting our analysis from Section 2.2, we can show they have the form

$$U_L(x) = \sum_{n \in \mathbb{Z}} (W(x+b+nL) - W(x-b+nL)) + I(x).$$

Applying the threshold conditions, $U_L(\pm b + nL) = \kappa$ then yields

$$(31) \qquad \sum_{n \in \mathbb{Z}} (W(2b+nL) - W(nL)) + I(b) = \mathbf{W}_L(b) + I(b) = G_L(b) = \kappa,$$

which defines an implicit equation for the half-width b of each active region. Local analysis can again be used to show that if there are any solutions to Eq. (31), the minimal one will be stable or marginally stable, since $G(x)$ will be decreasing or at a local minimum.

We now demonstrate that for a spatiotemporal input, $I(x,t) = I(x)\chi_{[0,t_1]}$, to generate a saturating solution, (i) Eq. (31) must have no solutions and (ii) t_1 must be large enough so the active region $A(t) = \cup_{n \in \mathbb{Z}}[-a(t)+nL, a(t)+nL]$ satisfies $a(t_1) > b_L$, where b_L solves Eq. (31) for $I \equiv 0$. Starting from $u_0(x) \equiv 0$, we know initially the dynamics obeys $\partial_t u(x,t) = -u(x,t) + I(x,t)$, so the time needed to produce a nontrivial active region is given by $t_0 = \ln\left[\frac{I(0)}{I(0)-\kappa}\right]$, as before. If $t_1 \leq t_0$, then the long term dynamics of the solution is $u(x,t) = I(x)(1 - \mathrm{e}^{-t_1})\mathrm{e}^{-(t-t_1)}$ for $t > t_1$, so $\lim_{t \to \infty} u(x,t) \equiv 0$. Note if $I(0) < \kappa$, then $u(x,t) < \kappa$ clearly for all $t > 0$.

If $t_1 > t_0$, then for $t_0 < t < t_1$, we can derive the interface equations for $u(\pm a(t), t) = \kappa$, similar to Eq. (26), finding

$$(32\mathrm{a}) \qquad a'(t) = -\frac{1}{\alpha(t)}\left[\mathbf{W}_L(a(t)) - \kappa + I(a(t))\right],$$

$$(32\mathrm{b}) \qquad \alpha(t) = u'_L(a(t))\mathrm{e}^{-t} + \mathrm{e}^{-t}\int_0^t \mathrm{e}^s \left[\sum_{n \in \mathbb{Z}} w_n(a(t), a(s)) + I(a(s))\right]\mathrm{d}s,$$

with initial conditions $a(t_0) = 0$ and $\alpha(t_0) = 0$, so $a'(t_0)$ diverges. As before, we can desingularize Eq. (32) with the change of variables $\tau = -\int_{t_0}^t \frac{\mathrm{d}s}{\alpha(s)}$, so we can write a differential equation for $\tilde{a}(\tau)$ in τ as

$$(33) \qquad \frac{\mathrm{d}\tilde{a}}{\mathrm{d}\tau} = \mathbf{W}_L(\tilde{a}(\tau)) - \kappa + I(\tilde{a}(\tau)),$$

with $\tilde{a}(0) = 0$. Since $\alpha(t) < 0$ for $t > t_0$, τ will be an increasing function of t, so we now refer to $\tau_1 := \tau(t_1)$ and note $\tau(t_0) = 0$. By assumption $I(0) - \kappa > 0$, so $\frac{\mathrm{d}\tilde{a}}{\mathrm{d}\tau} > 0$ for all τ where it is defined.
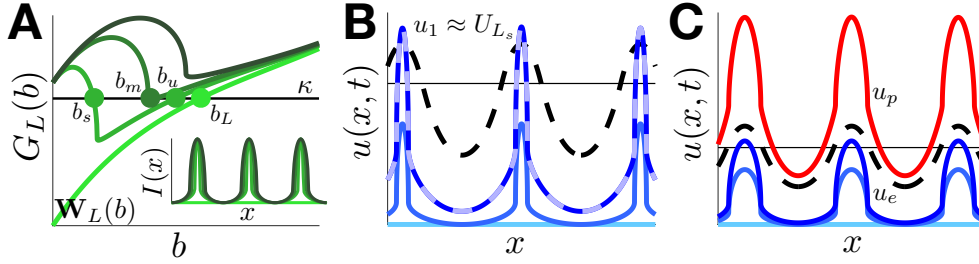
FIG. 9. *Conditions for propagation driven by a spatially-periodic input $I(x,t) = I(x)\chi_{[0,t_1]}$ with $I(x) = I(x + L)$, and $u(x,0) \equiv 0$. (A) For periodic, even, and positive profile $I(x)$ with $I(0) > \kappa$, propagation only occurs if $G_L(b) = \mathbf{W}_L(b) + I(b) = \kappa$ has no solutions. If solutions to Eq. (31) exist, the minimal one is linearly (b_s) or marginally (b_m) stable. For inputs $I(x)$ that are monotone decreasing on $x \in (0, L/2)$, there are only two solutions. (B) If $G_L(b_s) = \kappa$ is satisfied for some b_s, $u(x,t_1) \approx U_{L_s}(x)$ for large t_1 with active region centered at $x = 0$ given $[-a_s, a_s]$ where $a_s < b_L$, so $\lim_{t\to\infty} u(x,t) \equiv 0$. (C) Here $I(x)$ is chosen so that $G_L(b) = \kappa$ has no solutions. If $t_1 := t_e$, then $u_e(\pm a_e) := u(\pm a_e, t_e) = \kappa$ and $a_e < b_L$, so $\lim_{t\to\infty} u(x,t) \equiv 0$. However, for $t_1 := t_p$ with $u_p(\pm a_p) := u(\pm a_p, t_e) = \kappa$ and $a_p > b_L$, then $\lim_{t\to\infty} u(x,t) \equiv 1$.*

We now discuss the three remaining cases: (I) Eq. (31) has at least one solution, so saturation does not occur; (II) Eq. (31) has no solutions, but $\tau_1 \leq \tau_c$, the time at which $\tilde{a}(\tau_c) = b_L$ for $I(x, \tau) \equiv I(x)$, and saturation does not occur; (III) Eq. (31) has no solutions, and $\tau_1 > \tau_c$, so saturation occurs.

Case I: $\min_{x\in\mathbb{R}} G(x) \leq \kappa$. Here, Eq. (31) has at least one solution. Since we have assumed $I(0) > \kappa$, this solution $b_{\min}$ is linearly or marginally stable with respect to even and odd perturbations. Eq. (33) implies $\frac{d\tilde{a}}{d\tau} > 0$ for all $\tau < \tau_1$, but $\frac{d\tilde{a}}{d\tau}$ vanishes at $\tilde{a} = b_{\min}$, so $\tilde{a}(\tau) < b_{\min} < b_0$ for all $\tau < \tau_1$. Thus, once $\tau = \tau_1$, the dynamics is described by the extinction case from Section 4.2, and $\lim_{t\to\infty} u(x,t) \equiv 0$ (Fig. 9B).

Case II: $\min_{x\in\mathbb{R}} G(x) > \kappa$ *and* $\tau_1 \leq \tau_c$. Here Eq. (31) has no solutions, but $\tilde{a}(\tau)$ will not grow large enough for saturation to occur once $I(x,\tau) = 0$, since $\tau_1 \leq \tau_c$. We define τ_c as the critical time when $\tilde{a}(\tau_c) = b_L = \mathbf{W}_L^{-1}(\kappa)$, given by the formula

$$(34) \qquad \int_0^{\mathbf{W}_L^{-1}(\kappa)} \frac{\mathrm{d}a}{\mathbf{W}_L(a) - \kappa + I(a)} = -\int_{t_0}^{t_c} \frac{\mathrm{d}t}{\alpha(t)} := \tau_c.$$

By definition, $\tilde{a}(\tau_1) \leq b_L$, so once $\tau = \tau_1$, the dynamics is described by either (a) the extinction case in Section 4.2 if $\tau_1 < \tau_c$, so $\lim_{t\to\infty} u(x,t) \equiv 0$, or (b) the stagnation case in Section 4.2 if $\tau_1 = \tau_c$, so $\lim_{t\to\infty} u(x,t) \equiv U_L(x)$ (Fig. 9C).

Case III: $\min_{x\in\mathbb{R}} G(x) > \kappa$ *and* $\tau_1 > \tau_c$. Requiring $\tau_1 > \tau_c$ with Eq. (34), we have that $\tilde{a}(\tau_1) > b_L$. Thus, after $\tau = \tau_1$, the dynamics is described by the saturation case in Section 4.2, so $\lim_{t\to\infty} u(x,t) \equiv 1$ (Fig. 9C).

5. Discussion. In this paper, we have studied threshold phenomena of front propagation in the excitatory neural field Eq. (1) using an interface dynamics approach. Our interface analysis projects the dynamics of the integrodifferential equations to a set of differential equations for the boundaries of the active regions, where the neural activity is superthreshold. The interface equations can be used to categorize initial conditions or external stimuli based on whether the corresponding long term dynamics of the neural field are extinction ($u \to 0$), propagation/saturation ($u \to 1$), or stagnation ($u \to U_{\text{stat}}(x) \not\equiv 0, 1$). We considered several classes of initial conditions, which admit explicit results: (i) functions with a single active region; (ii) even and periodic functions with an infinite number of active regions; and (iii) a two-parameter family of even functions with two active regions. In these particular cases,

19

the conditions for extinction, propagation/saturation, or stagnation can be expressed in terms of a few inequalities for the parameters specifying the initial conditions. We were able to obtain a similar trichotomy when the neural field Eq. (1) is forced by a fixed critical stimulus (e.g., unimodal and periodic) over a finite time interval. Our analysis assumes the nonlinearity in the neural field arises from a Heaviside firing rate function, so the dynamics of the neural field Eq. (1) can be equivalently expressed as differential equations for the spatial locations where the neural activity equals the threshold of the firing rate function. This work addresses an important problem in the analysis of models of large-scale neural activity, determining the long term behavior of neuronal network dynamics that begin away from equilibrium.

There are several natural extensions of this work that build on the idea of developing critical thresholds for propagation in neural fields using an interface dynamics approach. For instance, one possibility would be to consider a planar version of Eq. (1), and develop closed form equations for the corresponding interface dynamics of the contours encompassing active regions as in [15]. In a preliminary analysis, we have already found that our results developed herein for single active regions can be extended to the case of radially symmetric initial conditions in two-dimensions (2D). Single stripe and periodic stripe patterns may also admit explicit analysis. However, there are also a number of other classes of initial condition that do not have a one-dimensional analogue, which could be interesting to explore, such as spot patterns and multiple concentric annuli. Employing our knowledge of the one-dimensional case may shed light on how to develop a theory for threshold phenomena in 2D. Alternatively, we may also consider neural fields with negative feedback that models adaptation [4, 22, 28, 31, 36], which are known to generate traveling pulses, spiral waves, or more exotic phenomena. In this case, the long term behavior of propagating solutions can be counter-propagating pulses rather than fronts.

REFERENCES

[1] J. Allard and A. Mogilner, *Traveling waves in actin dynamics and cell motility*, Current opinion in cell biology, 25 (2013), pp. 107–115.

[2] S. Amari, *Dynamics of pattern formation in lateral-inhibition type neural fields*, Biol. Cybern., 27 (1977), pp. 77–87.

[3] D. G. Aronson, *Density-dependent interaction–diffusion systems*, in Dynamics and modelling of reactive systems, Elsevier, 1980, pp. 161–176.

[4] D. Avitabile, M. Desroches, and E. Knobloch, *Spatiotemporal canards in neural field equations*, Physical Review E, 95 (2017), p. 042205.

[5] D. Avitabile and H. Schmidt, *Snakes and ladders in an inhomogeneous neural field model*, Physica D: Nonlinear Phenomena, 294 (2015), pp. 24–36.

[6] P. C. Bressloff, *Traveling fronts and wave propagation failure in an inhomogeneous neural network*, Physica D: Nonlinear Phenomena, 155 (2001), pp. 83–100.

[7] P. C. Bressloff, *Spatiotemporal dynamics of continuum neural fields*, Journal of Physics A: Mathematical and Theoretical, 45 (2012), p. 033001.

[8] P. C. Bressloff, J. D. Cowan, M. Golubitsky, P. J. Thomas, and M. C. Wiener, *Geometric visual hallucinations, euclidean symmetry and the functional architecture of striate cortex*, Philosophical Transactions of the Royal Society of London B: Biological Sciences, 356 (2001), pp. 299–330.

[9] S. Coombes, *Waves, bumps, and patterns in neural field theories*, Biological cybernetics, 93

(2005), pp. 91–108.

[10] S. COOMBES AND C. LAING, *Pulsating fronts in periodically modulated neural field models*, Physical Review E, 83 (2011), p. 011912.

[11] S. COOMBES, G. J. LORD, AND M. R. OWEN, *Waves and bumps in neuronal networks with axo-dendritic synaptic interactions*, Physica D: Nonlinear Phenomena, 178 (2003), pp. 219–241.

[12] S. COOMBES AND M. OWEN, *Bumps, breathers, and waves in a neural network with spike frequency adaptation*, Physical Review Letters, 94 (2005), p. 148102.

[13] S. COOMBES AND M. R. OWEN, *Evans functions for integral neural field equations with heaviside firing rate function*, SIAM Journal on Applied Dynamical Systems, 3 (2004), pp. 574–600.

[14] S. COOMBES AND H. SCHMIDT, *Neural fields with sigmoidal firing rates: approximate solutions*, Discrete and Continuous Dynamical Systems. Series S, 28 (2010), pp. 1369–1379.

[15] S. COOMBES, H. SCHMIDT, AND I. BOJAK, *Interface dynamics in planar neural field models*, J Math Neurosci, 2 (2012), p. 9, https://doi.org/10.1186/2190-8567-2-9.

[16] K. DELANEY, A. GELPERIN, M. FEE, J. FLORES, R. GERVAIS, D. TANK, AND D. KLEINFELD, *Waves and stimulus-modulated dynamics in an oscillating olfactory network.*, Proceedings of the National Academy of Sciences, 91 (1994), pp. 669–673.

[17] Y. DU AND H. MATANO, *Convergence and sharp thresholds for propagation in nonlinear diffusion problems*, Journal of the European Mathematical Society, 12 (2010), pp. 279–312.

[18] B. ERMENTROUT, *Neural networks as spatio-temporal pattern-forming systems*, Reports on progress in physics, 61 (1998), p. 353.

[19] G. B. ERMENTROUT AND J. B. MCLEOD, *Existence and uniqueness of travelling waves for a neural network*, Proceedings of the Royal Society of Edinburgh Section A: Mathematics, 123 (1993), pp. 461–478.

[20] J. FANG AND G. FAYE, *Monotone traveling waves for delayed neural field equations*, Mathematical Models and Methods in Applied Sciences, 26 (2016), pp. 1919–1954.

[21] G. FAYE, *Existence and stability of traveling pulses in a neural field equation with synaptic depression*, SIAM Journal on Applied Dynamical Systems, 12 (2013), pp. 2032–2067.

[22] G. FAYE AND A. SCHEEL, *Existence of pulses in excitable media with nonlocal coupling*, Advances in Mathematics, 270 (2015), pp. 400–456.

[23] I. FEREZOU, S. BOLEA, AND C. C. PETERSEN, *Visualizing the cortical representation of whisker touch: voltage-sensitive dye imaging in freely moving mice*, Neuron, 50 (2006), pp. 617–629.

[24] S. E. FOLIAS AND P. C. BRESSLOFF, *Breathing pulses in an excitatory neural network*, SIAM Journal on Applied Dynamical Systems, 3 (2004), pp. 378–407.

[25] X. GAO, W. XU, Z. WANG, K. TAKAGAKI, B. LI, AND J.-Y. WU, *Interactions between two propagating waves in rat visual cortex*, Neuroscience, 216 (2012), pp. 57–69.

[26] B. GRENFELL, O. BJØRNSTAD, AND J. KAPPEY, *Travelling waves and spatial hierarchies in measles epidemics*, Nature, 414 (2001), pp. 716–723.

[27] F. HAN, N. CAPORALE, AND Y. DAN, *Reverberation of recent visual experience in spontaneous cortical waves*, Neuron, 60 (2008), pp. 321–327.

[28] X. HUANG, W. C. TROY, Q. YANG, H. MA, C. R. LAING, S. J. SCHIFF, AND J.-Y. WU, *Spiral waves in disinhibited mammalian neocortex*, Journal of Neuroscience, 24 (2004), pp. 9897–9902.

[29] X. HUANG, W. XU, J. LIANG, K. TAKAGAKI, X. GAO, AND J.-Y. WU, *Spiral wave dynamics in neocortex*, Neuron, 68 (2010), pp. 978–990.

[30] A. HUTT, M. BESTEHORN, AND T. WENNEKERS, *Pattern formation in intracortical neuronal fields*, Network: Computation in Neural Systems, 14 (2003), pp. 351–368.

[31] Z. P. KILPATRICK AND P. C. BRESSLOFF, *Effects of synaptic depression and adaptation on spatiotemporal dynamics of an excitatory neuronal network*, Physica D: Nonlinear Phenomena, 239 (2010), pp. 547–560.

[32] K. KOLODINA, V. KOSTRYKIN, AND A. OLEYNIK, *Existence and stability of periodic solutions in a neural field equation*, arXiv preprint arXiv:1712.09688, (2017).

[33] N. KRISHNAN, D. B. POLL, AND Z. P. KILPATRICK, *Synaptic efficacy shapes resource limitations in working memory*, Journal of computational neuroscience, (2018), pp. 1–23.

[34] C. R. LAING, W. C. TROY, B. GUTKIN, AND G. B. ERMENTROUT, *Multiple bumps in a neuronal model of working memory*, SIAM Journal on Applied Mathematics, 63 (2002), pp. 62–97.

[35] J. D. MURRAY, *Mathematical Biology*, Springer-Verlag New York Incorporated, 2001.

[36] D. J. PINTO AND G. B. ERMENTROUT, *Spatially structured activity in synaptically coupled neuronal networks: I. traveling fronts and pulses*, SIAM journal on Applied Mathematics, 62 (2001), pp. 206–225.

[37] K. A. RICHARDSON, S. J. SCHIFF, AND B. J. GLUCKMAN, *Control of traveling waves in the mammalian cortex*, Physical review letters, 94 (2005), p. 028103.

[38] I. M. ROUZINE, J. WAKELEY, AND J. M. COFFIN, *The solitary wave of asexual evolution*, Proceedings of the National Academy of Sciences, 100 (2003), pp. 587–592.

[39] T. K. SATO, I. NAUHAUS, AND M. CARANDINI, *Traveling waves in visual cortex*, Neuron, 75 (2012), pp. 218–229.

[40] W. C. TROY AND V. SHUSTERMAN, *Patterns and features of families of traveling waves in large-scale neuronal networks*, SIAM Journal on Applied Dynamical Systems, 6 (2007), pp. 263–292.

[41] X.-J. WANG, *Neurophysiological and computational principles of cortical rhythms in cognition*, Physiological reviews, 90 (2010), pp. 1195–1268.

[42] H. R. WILSON AND J. D. COWAN, *A mathematical theory of the functional dynamics of cortical and thalamic nervous tissue*, Biological Cybernetics, 13 (1973), pp. 55–80.

[43] J.-Y. WU, X. HUANG, AND C. ZHANG, *Propagating waves of activity in the neocortex: what they are, what they do*, The Neuroscientist, 14 (2008), pp. 487–502.

[44] W. XU, X. HUANG, K. TAKAGAKI, AND J.-Y. WU, *Compression and reflection of visually evoked cortical waves*, Neuron, 55 (2007), pp. 119–129.

[45] A. ZLATOŠ, *Sharp transition between extinction and propagation of reaction*, Journal of the American Mathematical Society, 19 (2006), pp. 251–263.